2017

Pontryagin Principle Applied to Commercial Aircrafts Optimal Control Problem under Physical and Energetic Constraints

Nahayo, Fulgence

ICSRS Publication

Gen. Math. Notes, Vol. 38, No. 1, 2017, pp.1-xx
ISSN 2219-7184; Copyright ©ICSRS Publication, 2017
www.i-csrs.org
Available free online at http://www.geman.in

Pontryagin Principle Applied to Commercial Aircrafts Optimal Control Problem under Physical and Energetic Constraints

Dr. Fulgence Nahayo[1,2]

[1]Burundi University, Engineering Sciences Faculty, P.O. Box–2720, Bujumbura
[2]ENA, Computer Sciences Department, P.O. Box–780, Bujumbura, Burundi
E-mail: nahayo.fulgence@gmail.com

(Received: 3-8-16/ Accepted: 22-6-17)

Abstract

The objective of this work is the development of a control and optimization flight paths model minimizing fuel consuption and noise perceived on the ground for two aircraft when flight constraints are considered. Flight dynamics, combined with the criterion to minimize noise levels generates an optimal control problem governed by nonlinear differential equations . This problem is solved using an indirect method applying the minimum principle of Pontryagin and a dynamic programming method. Obtained optimal results showed significant reductions of fuel consumption and noise levels. This model shows and confirm environmental Approach impact around airport by reduction of the gene for neighbors due to noise. Reduction of Economic cost to airlines and for builders are also confirmed. An optimal approach path when compared to standard flight path is confirmed.This model can be generalized for any type of aircraft when considering real case for airport trafic and air traffic.

Keywords: *Aircraft, Mathematical Modeling, Control Theory, Optimisation, Noise, Fuel Consumption, SPRK4 Algorithm, AMPL, KNITRO Solver.*

1 Introduction

Considering the current strong growth of air transportation [1, 2], economic and environmental considerations related to the increase in oil prices and the

need to preserve the environment impose strong constraints for the design of future generations of aircraft. These constraints are based on the ACARE objectives, which suggest a 50% reduction perceived noise in 2020 [3]. Reaching this goal is a real scientific and technical challenge when considering the aerodynamic, acoustic optimization and mathematical modeling side. Some existing models in the literature deal with minimizing the noise of a commercial airplane in physical and aerodynamic constraints [4, 5]. Others treat the optimization of operational procedures reducing noise, stochastic conflict detection for air traffic and the performance and optimization of the movement of planes on an airport [5, 6, 7]. However, in this work, the noise optimization is limited to the case of a single flight. The objectives in this work concerning the development of a theoretical model of noise optimization taking into account the evolution of flight procedures of two commercial aircraft approach. Numerically considerations for solving a mathematical model of a nonlinear optimization problem are applied. This model is a nonlinear optimal control and non-convex [8] as governed by a system of ordinary differential equations. The numerical considerations used have no limitations except the introduction of the costate-variables without physical interpretation in order to facilitate the resolution of the dynamic system of two airplanes. The reason is the complexity of this system, which greatly affects the nature of the Solver to use. In this paper, the solver was chosen in consideration of all these parameters.
This model can be generalized for any type of aircraft when considering real case for airport trafic.

2 Mathematical modeling

The motion of each plane $A_i, i := 1, 2$ is three dimensional analyzed with 3 frames : the landmark $(O, \overrightarrow{X}_1, \overrightarrow{Y}_1, \overrightarrow{Z}_1)$, the plane frame $(G_i, \overrightarrow{X}_{Gi}, \overrightarrow{Y}_{Gi}, \overrightarrow{Z}_{Gi})$ and the aerodynamic one $(G_i, \overrightarrow{X}_{ai}, \overrightarrow{Y}_{ai}, \overrightarrow{Z}_{ai})$. The transition between these three frames is shown easily with three successive rotations. In general, the equations of motion of each aircraft are summarized in two basic relations of mechanics and the fundamental relationship of kinematics: [9]:

$$\begin{array}{l} \sum F_{ext_i} - \frac{dm_i}{dt}\overrightarrow{V_i} = \frac{m_i d\overrightarrow{V}_i}{dt} \\ \sum M_{ext_{G_i}} = J(G_i, A_i)\frac{d\Omega_i}{dt} \\ \frac{d\overrightarrow{X}^o}{dt} = \frac{d\overrightarrow{X}^1}{dt} + \Omega_{10} \times \overrightarrow{X} \end{array} \tag{1}$$

In the system above, F_{ext_i}represent the external forces acting on the aircraft, $m_i(t)$ the mass of the aircraft, V_i the airspeed of aircraft, $M_{ext_{G_i}}$ the outside moments of each aircraft, $J(G_i, A_i)$ the inertia matrix and Ω_i the angular rotation.

The mathematical modelisation considerations show the following system

$$
\begin{cases}
\dot{m}_i = -2.01\times10^{-5}\dfrac{(\Phi-\mu_i-\frac{K_i}{\eta_c})\sqrt{\Theta}}{\sqrt{5\eta_n(1+\eta_{tf_i}\lambda)}\sqrt{G_i+0.2M_i^2\frac{\eta_{d_i}}{\eta_{tf_i}}\lambda-(1-\lambda)M_i}}P_0\delta_{xi}\dfrac{\rho_i}{\rho_0}(1-M_i+\dfrac{M_i^2}{2}),\\
\dot{V_{a_i}} = \dfrac{1}{m_i}[-m_igsin\gamma_{a_i}-\dfrac{1}{2}\rho_iSV_{a_i}^2C_{D_i}+(cos\alpha_{a_i}cos\beta_{a_i}+sin\beta_{a_i}+sin\alpha_{a_i}cos\beta_{a_i})F_{x_i}-\dfrac{dm_i}{dt}u_i-m_i\Delta A_u^i],\\
\dot{\beta_{a_i}} = \dfrac{1}{m_iV_{a_i}}[m_igcos\gamma_{a_i}sin\mu_{a_i}+\dfrac{1}{2}\rho_iSV_{a_i}^2C_{y_i}+[-cos\alpha_{a_i}sin\beta_{a_i}+cos\beta_{a_i}-sin\alpha_{a_i}sin\beta_{a_i}]F_{y_i}\\
-\dfrac{dm_i}{dt}v_i-m_i\Delta A_v^i],\\
\dot{\alpha_{a_i}} = \dfrac{1}{m_iV_{a_i}cos\beta_{a_i}}[m_igcos\gamma_{a_i}cos\mu_{a_i}-\dfrac{1}{2}\rho_iSV_{a_i}^2C_{L_i}+[-sin\alpha_{a_i}+cos\alpha_{a_i}]F_{z_i}-\dfrac{dm_i}{dt}w_i-m_i\Delta A_w^i],\\
\dot{p}_i = \dfrac{C}{AC-E^2}\{r_iq_i(B-C)-Ep_iq_i+\dfrac{1}{2}\rho_iSlV_{a_i}^2C_{l_i}+\sum_{j=1}^{2}F_j[y_{M_ij}^bcos\beta_{m_ij}sin\alpha_{m_ij}-z_{M_ij}^bsin\beta_{m_ij}]\}\\
+\dfrac{E}{AC-E^2}\{p_iq_i(A-B)-Er_iq_i+\dfrac{1}{2}\rho_iSlV_{a_i}^2C_{ni}+\sum_{j=1}^{2}F_j[x_{M_ij}^bsin\beta_{m_ij}-y_{M_ij}^bcos\beta_{m_ij}cos\alpha_{m_ij}]\},\\
\dot{q}_i = \dfrac{1}{B}\{-r_ip_i(A-C)-E(p_i^2-r_i^2)+\dfrac{1}{2}\rho_iSlV_{a_i}^2C_{mi}+\sum_{j=1}^{2}F_j[z_{M_ij}^bcos\beta_{m_ij}cos\alpha_{m_ij}-x_{M_ij}^bcos\beta_{m_ij}sin\alpha_{m_ij}]\},\\
\dot{r}_i = \dfrac{E}{AC-E^2}\{r_iq_i(B-C)+Ep_iq_i+\dfrac{1}{2}\rho_iSlV_{a_i}^2C_{l_i}+\sum_{j=1}^{2}F_j[y_{M_ij}^bcos\beta_{m_ij}sin\alpha_{m_ij}-z_{M_ij}^bsin\beta_{m_ij}]\}\\
+\dfrac{A}{AC-E^2}\{p_iq_i(A-B)-Er_iq_i+\dfrac{1}{2}\rho_iSlV_{a_i}^2C_{ni}+\sum_{j=1}^{2}F_j[x_{M_ij}^bsin\beta_{m_ij}-y_{M_ij}^bcos\beta_{m_ij}cos\alpha_{m_ij}]\},\\
\dot{X}_{G_i} = V_{a_i}cos\gamma_{a_i}cos\chi_{a_i}+u_w,\\
\dot{Y}_{G_i} = V_{a_i}cos\gamma_{a_i}sin\chi_{a_i}+v_w,\\
\dot{Z}_{G_i} = -V_{a_i}sin\gamma_{a_i}+w_w,\\
\dot{\phi}_i = p_i+q_isin\phi_itan\theta_i+r_icos\phi_itan\theta_i,\\
\dot{\theta}_i = q_icos\phi_i-r_isin\phi_i,\\
\dot{\psi}_i = \dfrac{sin\phi_i}{cos\theta_i}q_i+\dfrac{cos\phi_i}{cos\theta_i}r_i
\end{cases}
\tag{2}
$$

$j\in\{1,2\}$ means i aircraft engines, $A=I_{xx}, B=I_{yy}, C=I_{zz}, E=I_{xz}$ are are the inertia moments of the 2 aircrafts, ρ_i is air density, S aircraft reference aria, l is the aircraft reference length, g acceleration due to gravity, $C_{D_i}=C_{D0}+kC_{Li}^2$ is the drag coefficient, $C_{yi}=C_{y\beta}\beta+C_{yp}\frac{pl}{V}+C_{yr}\frac{rl}{V}+C_{Y\delta_l}\delta_{li}+C_{Y\delta_n}\delta_{ni}$ is the lateral forces coefficient, $C_{Li}=C_{L\alpha}(\alpha_a-\alpha_{a0})+C_{L\delta_m}\delta_{mi}+C_{LM}M_i+C_{Lq}\frac{q_a^bl}{V}$ is the lifft forces coefficient,, $C_{li}=C_{l\beta}\beta+C_{lp}\frac{pl}{V}+C_{lr}\frac{rl}{V}+C_{l\delta_l}\delta_{li}+C_{l\delta_n}\delta_{ni}$ is the rolling moment coefficient, $C_{mi}=C_{m0}+C_{m\alpha}(\alpha-\alpha_0)+C_{m\delta_m}\delta_{mi}$ is the pitching moment coefficient, $C_{ni}=C_{n\beta}\beta+C_{np}\frac{pl}{V}+C_{nr}\frac{rl}{V}+C_{n\delta_l}\delta_{li}+C_{n\delta_n}\delta_{ni}$ is the yawing moment coefficient, $(x_{Mij}^b, x_{Mij}^b, x_{Mij}^b)$ is engine position, P_0 is the full thrust, ρ_0 is the atmospheric density at the ground, $F=(F_{xi},F_{yi},F_{zi})$ is the propulsive force, $V_{ai}=(u_i,v_i,w_i)$ is the aerodynamic speed, $(\Delta A_u^i,\Delta A_v^i,\Delta A_w^i)$ is complementary acceleration, (u_w,v_w,w_w) is wind speed, β_{mij} is engine yaw control, α_{mij} engine picth control. The mass variation is reflected in the fuel consumption of the aircraft as described by E. Torenbeek where specific consumption is

$$
C_{SR_i}=2.01\times10^{-5}\frac{(\Phi-\mu_i-\frac{K_i}{\eta_c})\sqrt{\Theta}}{\sqrt{5\eta_n(1+\eta_{tf_i}\lambda)}\sqrt{G_i+0.2M_i^2\frac{\eta_{d_i}}{\eta_{tf_i}}\lambda-(1-\lambda)M_i}} \tag{3}
$$

$$G_i = (\Phi - \frac{K_i}{\eta_c})(1 - \frac{1.01}{\eta_i^{\frac{\nu-1}{\nu}}(K_i + \mu_i)(1 - \frac{K_i}{\Phi\eta_c\eta_t})}), K_i = \mu_i(\epsilon_c^{\frac{\nu-1}{\nu}} - 1), \mu_i = 1 + \frac{\nu-1}{2}M_i^2 \tag{4}$$

is the power function gas generator. Nomenclature engine performance variables is given by G_i. G0 power function gas generator (static, at sea level), K temperature function for compression process, M_i Mach Number of flight, T4 Total temperature at turbine entry, T0 real temperature at the level of the sea. T flight temperature, the nomenclature engine performances is $\eta_c = 0.85$ isentropic efficiency of the compressor, $\eta_{d_i} = 1 - 1.3(\frac{0.05}{Re^{\frac{1}{5}}})^2(\frac{0.5}{M_i})^2\frac{L}{D}$, the isentropic efficiency of the fan inlet duct, L the length of the duct, D input diameter, Re the Reynolds number at the entrance to the nozzle, $\eta_{f_i} = 0.86 - 3.13 \times 10^{-2}M_i$ Performance isentropic fan. $\eta_i = \frac{1 + \eta_d\frac{\gamma-1}{2}M_i^2}{1 + \frac{\gamma-1}{2}M_i^2}$ the gas Generator intake stagnation pressure ratio, $\eta_n = 0.97$ the isentropic efficiency of the expansion process in the nozzle, $\eta_t = 0.88$ the efficiency of the isentropic turbine. $\eta_{tf_i} = \eta_t\eta_f$, ϵ_c the overall pressure ratio (compressor). ν the ratio of specific heats $\nu = 1.4$, λ dilution ratio, μ_i the ratio of the stagnation in the static temperature of the ambient air. Φ the temperature at the inlet of the non-dimensional turbine $\Phi = \frac{T_4}{T}$ and $\Theta = \frac{T}{T_0}$ the relative ambient temperature .

The expressions $\alpha_{ai}(t), \beta_{ai}(t), \theta_i(t), \psi_i(t), \phi_i(t), V_{a_i}(t), X_{G_i}(t), Y_{G_i}(t), Z_{G_i}(t)$, $p_i(t), q_i(t), r_i(t), m_i(t)$ are respectively the attack angle, the aerodynamic sideslip angle, the inclination angle, the cup, the roll angle, the airspeed, the position vectors, the roll velocity of the aircraft relative to the earth, the pitch velocity of the aircraft relative to the earth, the yaw velocity of the aircraft relative to the earth and the aircraft mass.

Mathematical modelisation of equations system (2) show

$$\begin{aligned} \frac{d\mathbf{y}_i(t)}{dt} &= \mathbf{f}_i(\mathbf{y}_i(t), \mathbf{u}_i(t)), \\ \mathbf{y}_i(t) &= (\alpha_{ai}(t), \beta_{ai}(t), \theta_{ai}(t), \psi_{ai}(t), \phi_i(t), V_{a_i}(t), X_{G_i}(t), Y_{G_i}(t), Z_{G_i}(t), p_i(t), \\ &\quad q_i(t), r_i(t), m_i(t)) \\ \mathbf{u}_i(t) &= (\delta_{l_i}(t), \delta_{m_i(t)}, \delta_{n_i}(t), \delta_{x_i}(t)). \end{aligned} \tag{5}$$

where $\mathbf{y}_i$ is called state function and expressions $\delta_{l_i}(t), \delta_{m_i(t)}, \delta_{n_i}(t), \delta_{x_i}(t)$ are respectively roll control, pitch control, yaw control and thrust control of each aircraft. The dynamics relationship can be written as: $\dot{\mathbf{y}}_i(t) = \mathbf{f}_i(\mathbf{y}_i, \mathbf{u}_i, t), \forall t \in [0, T], y_i(0) = y_{i0}$.

The objective function model

Let use the Sound Exposure Level (SEL)or the fuel consumption Torenbeek model as cost functions. The Sound Exposure Level:

$$SEL = 10log\left[\frac{1}{t_o}\int_t\left(\frac{P^2_{Aeff}}{P^2_{ref}}\right)dt'\right], \tag{6}$$

where t the noise event interval and $t_o = 1\ s$ the time reference , P^2_{Aeff}, P^2_{ref} are effective pression and reference pression.

$$\begin{aligned}
SEL_1 &= 10log\left[\frac{1}{t_o}\int_{t_{10}}^{t_{20}} 10^{0.1L_{A1,dt}(t)}dt\right], t\in[t_{10},t_{20}]\\
SEL_{12} &= SEL_{11}\oplus SEL_{21}\\
&= 10\log\left[\frac{1}{t_o}\int_{t_{20}}^{t_{1f}} 10^{0.1L_{A1,dt}(t)}dt + \frac{1}{t_o}\int_{t_{20}}^{t_{1f}} 10^{0.1L_{A2,dt}(t)}dt\right], t\in[t_{20},t_{1f}]\\
SEL_2 &= 10\log\left[\frac{1}{t_o}\int_{t_{20}}^{t_{2f}} 10^{0.1L_{A2,dt}(t)}dt\right], t\in[t_{1f},t_{2f}]\\
SEL_G &= \frac{(t_{20}-t_{10})\,SEL_1\oplus(t_{1f}-t_{20})\,SEL_{12}\oplus(t_{2f}-t_{1f})\,SEL_2}{t_{2f}-t_{10}}\\
&= 10\log\{\frac{1}{t_{2f}-t_{10}}[(t_{20}-t_{10})\int_{t_{10}}^{t_{20}} 10^{0.1L_{A1}(t)}dt\\
&+(t_{1f}-t_{20})\int_{t_{20}}^{t_{1f}} 10^{0.1L_{A1}(t)}dt + (t_{1f}-t_{20})\int_{t_{20}}^{t_{1f}} 10^{0.1L_{A2}(t)}dt\\
&+(t_{2f}-t_{1f})\int_{t_{1f}}^{t_{2f}} 10^{0.1L_{A2}(t)}dt,]\}, t\in[t_{10},t_{2f}]
\end{aligned} \tag{7}$$

where SEL_G is the global noise of two aircraft and $\oplus$ is sound adding operator.

Expression $L_{A1}(t)$ is first aircraft jet noise given by the formula [4] :

$$L_{A1}(t) = 141+10\log\left(\frac{\rho_1}{\rho}\right)^w+10\log\left(\frac{V_e}{c}\right)^{7.5}+10\log s_1+3\log\left(\frac{2s_1}{\pi d_1^2}+0.5\right)+$$

$$5\log\frac{\tau_1}{\tau_2}+10\log\left[\left(1-\frac{v_2}{v_1}\right)^{me}+1.2\frac{\left(1+\frac{s_2v_2^2}{s_1v_1^2}\right)^4}{\left(1+\frac{s_2}{s_1}\right)^3}\right]-20\log R+\Delta V$$

$$+10\log\left[\left(\frac{\rho}{\rho_{ISA}}\right)^2\left(\frac{c}{c_{ISA}}\right)^4\right],$$ where v_1 is the jet speed at the entrance of the nozzle, v_2 the jet speed at the nozzle exit, τ_1 the inlet temperature of the nozzle, τ_2 the temperature at the nozzle exit, ρ the density of air, ρ_1 the atmospheric density at the entrance of the nozzle, ρ_{ISA} the atmospheric density at ground, s_1 the en- trance area of the nozzle hydraulic engine, s_2 the emitting surface of the nozzle hydraulic engine, d_1 the inlet diameter of the nozzle hydraulic engine, $V_e = v_1[1-(V/v_1)\cos(\alpha_p)]^{2/3}$ the effective speed , α_p is the angle between the axis of the motor and the axis of the aircraft, R the source observer distance, $w = \dfrac{3(V_e/c)^{3.5}}{0.6+(V_e/c)^{3.5}} - 1$ is the exponent variable, c is the sound velocity (m/s), me the exhibiting variable depending on

the type of aircraft, $me = 1.1\sqrt{\frac{s_2}{s_1}}$; $\frac{s_2}{s_1} < 29.7$, $me = 6.0$; $\frac{s_2}{s_1} \geq 29.7$, $\Delta V = -15log(C_D(M_c, \theta)) - 10log(1 - Mcos\theta)$ means the Doppler convection when $C_D(M_c, \theta) = [(1 + M_c cos\theta)^2 + 0.04M_c^2]$, M the aircraft Mac Number, $M_c = 0.62(v_1 - Vcos(\alpha_p))/c$ the convection Mac Number, θ is the Beam angle.

The cost function: Considering the formula (7), the cost function become: $J_{12}(y(t), u(t), i = 1, 2) = \int_{t'} g(y(t), u(t), t)dt$ où $J_{12}(y(t), u(t), t) = SEL_G$ is the global noise of the two aircraft.

Constraints: Constraints are the security constraints, speed, altitude, angle of attack, roll angle, yaw angle, the position of the throttle, the energy constraint, longitudinal and vertical separation of aircraft. Some constraints are shared by the two aircraft, others are individual. Shared constraints are vertical separation $h_{12} = h_2 - h_1$ where h_1, h_2 are respectively altitude of the first and the second aircraft, The horizontal separation $x_{12} = x_1 - x_2$ [10, 11, 12] where x_1, x_2 are aircraft horizontal separation. The time separation $t_{20} - t_{10} = t_{2f} - t_{1f}$ varies from 45 s to 90 s where t_{10} is the start time of the approach of the first plane and t_{20} for the second aircraft. These are reflected in the boundary conditions.
Both aircraft are landing on one track [13]. The aircraft speeds V_i are bound as $1.13V_s \leq V_i \leq V_f$ where V_s is stall speed, V_f the maximum speed of the aircraft A_i during approach phase[14, 15].
During approch phase, The slope required by OACI is $\gamma_i \in [\gamma_0, \gamma_f]$. For flight angles, the angle of attack is $\alpha_i \in [\alpha_o, \alpha_f]$, the roll angle $\mu_i \in [\mu_o, \mu_f]$ and the yaw angle $\chi_i \in [\chi_o, \chi_f]$. The throttle δ_{xi} oscillates between positions δ_{xo} and δ_{xf}. The A_i aircraft mass is $m_i \in [m_o, m_f]$ when considering aircraft fuel consumption [16, 17].
Functional all constraints is written:

$$\begin{array}{l} a \leq C(y_i(t), u_i(t), t) \leq b \\ C(t) : \mathbf{R^7} \times \mathbf{R^3} \times \mathbf{R} \longrightarrow \mathbf{R^{10}}, \\ (y_i(t), u_i(t), t) \longrightarrow C(y_i(t), u_i(t), t). \end{array} \tag{8}$$

The exact values of these constraints are contained in Table 1 in the Appendix. The index 1 means the 1^{st} plane and index 2 the 2^{nd} plane.

Considering equations equations (5), (7), (8), the optimisation problem

becomes :

$$\begin{cases} \min_{(y,u)\in \mathbf{Y}\times\mathbf{U}} J_{12}(y(t),u(t)) = \int_{t10}^{t_{1f}} g_1(y_1(t),u_1(t),t)dt + \\ \int_{t20}^{t_{1f}} g_{12}(y_1(t),u_1(t),y_2(t),u_2(t),t)dt + \int_{t20}^{t_{2f}} g_2(y_2(t),u_2(t),t)dt + \phi(y(t_f)) \\ \dot{y}(t) = f(u(t),y(t)), u(t) = (u_1(t),u_2(t)), y(t) = (y_1(t),y_2(t)), \\ \forall t \in [t_{10},t_{2f}], t_{10} = 0, \\ y(0) = y_0, y(t_f) = y_T, u(0) = u_0, \\ a \leq C(y(t),u(t)) \leq b. \end{cases} \tag{9}$$

Constraints equations can be modelized as:

$$a \leq C(y(t),u(t)) \leq b \equiv \begin{cases} a - C(y(t),u(t)) \leq 0 \\ b - C(y(t),u(t)) \geq 0, \end{cases} \tag{10}$$

.In the following we apply the Pontryagin minimum principe.

3 Solving Algorithm Development

The system (9) is an optimal control problem with mixed constraints on the state and control. In order to apply the formulation of Pontryagin, we rewrite directly this system as follows:

$$\begin{cases} \min J_{12}(y,u) = \int_{t0}^{t_f} g(y(t),u(t),t)dt \\ \dot{y}(t) = F(y(t),u(t)) \\ k_1(y,u,t) \leq 0, \\ k_2(y,u,t) \geq 0, \end{cases} \tag{11}$$

where

$$\begin{array}{ll} k_{1i}(\mathbf{y}_i,\mathbf{u}_i) & \leq 0, k_{2i}(\mathbf{y}_i,\mathbf{u}_i) \geq 0 \\ k_{1i}(\mathbf{y}_i,\mathbf{u}_i) & = (\alpha_i(t) - \alpha_{if}, \theta_i(t) - \theta_{if}, \psi_i(t) - \psi_{if}, \phi_i(t) - \phi_{if}, V_{a_i}(t) - V_{aif}, \\ & X_{G_i}(t) - X_{Gif}, Y_{G_i}(t) - Y_{Gif}, Z_{G_i}(t) - Z_{Gif}, p_i(t) - p_{if}, q_i(t) - q_{if}, \\ & r_i(t) - r_{if}, \delta_{l_i}(t) - \delta_{l_if}, \delta_{m_i}(t) - \delta_{mif}, \delta_{n_i}(t) - \delta_{nif}, \delta_{x_i}(t) - \delta_{xif}, \\ & m_i(t) - m_{if}), \\ k_{2i}(\mathbf{y}_i,\mathbf{u}_i) & = (\alpha_i(t) - \alpha_{i0}, \theta_i(t) - \theta_{i0}, \psi_i(t) - \psi_{i0}, \phi_i(t) - \phi_{i0}, V_{a_i}(t) - V_{ai0}, \\ & X_{G_i}(t) - X_{Gi0}, Y_{G_i}(t) - Y_{Gi0}, Z_{G_i}(t) - Z_{Gi0}, p_i(t) - p_{i0}, q_i(t) - q_{i0}, \\ & r_i(t) - r_{i0}, \delta_{l_i}(t) - \delta_{l_i0}, \delta_{m_i}(t) - \delta_{mi0}, \delta_{n_i}(t) - \delta_{ni0}, \delta_{x_i}(t) - \delta_{xi0}, \\ & m_i(t) - m_{i0}). \end{array}$$

The Runge-Kutta discretization of this system gives

$$\begin{cases} \min\limits_{u_{n_k}} J_{12}(y_n, u_{n_k}) \\ y_{n+1} = y_n + h\sum\limits_{k=1}^{s} b_k F(y_{n_k}, u_{n_k}), y(t_0) = y_0 \\ y_{n_k} = y_n + h\sum\limits_{j=1}^{s} a_k j F(y_{n_j}, u_{n_j}), k = 1, ..., s \\ k_1(y_n, u_{n_k}) \leq 0, \\ k_2(y_n, u_{n_k}) \geq 0, \end{cases} \tag{12}$$

where h is the integration step.

On the other hand, let us consider the pseudo-Hamiltonian system (11) given by

$$\mathbf{H}(y, u, p, p_0, t) = p^T F(y, u, t) - p_0 g(y, u, t) - \mu_1 k_1(y, u, t) - \mu_2 k_2(y, u, t) \tag{13}$$

with $p = (p_1, p_2), p_i = (p_{1i}, p_{2i}, p_{3i}, p_{4i}, p_{5i}, p_{6i}, p_{7i}, p_{8i}, p_{9i}, p_{10i}, p_{11i}, p_{12i}, p_{13i})^T$ the adjoint state. With this new formulation of Pontryagin, the necessary optimality conditions are given by

$$\begin{array}{l} \mathbf{H_u}(y, u, p, p_0, t) = 0 \\ \dot{y} = \mathbf{H_p}(y, u, p, p_0, t) = F(y(t), u(t)) \\ \dot{p} = -\mathbf{H_y}(y, u, p, p_0, t) \\ k_1(y, u, t) \leq 0, k_2(y, u, t) \geq 0, t \in [t_0, t_f], \mu_2 \geq 0, \end{array} \tag{14}$$

where H is pseudo-hamiltonon system. Considering equation $\mathbf{H_u}(y, u, p, p_0, t) = 0$, Under certain regularity assumptions, we have:

$$u(t) = \psi(y(t), p(t)). \tag{15}$$

Hamimitonon system is

$$\mathcal{H}(y, u, p, p_0, t) = H(\psi(y, p), y, p). \tag{16}$$

That's why

$$\begin{array}{l} \dot{y} = \mathcal{H}_p(y, u, p, p_0, t), y(t_0) = y_0 \\ \dot{p} = -\mathcal{H}_y(y, u, p, p_0, t), p(t_f) = \phi'(y(t_f)) \\ k_1(y, u, t) \leq 0, k_2(y, u, t) \geq 0, t \in [t_0, t_f], \end{array} \tag{17}$$

The above system is a Hamiltonian system. The conservation of the Hamiltonian is not guaranteed along digital solutions like the digital stream is not symplectic. Using Lagrange, a curve $y_n, p_n, u_{n_k}, q_{n_k}$ is an optimal solution of the problem

$$\begin{cases} \min\limits_{u_{n_k}} J_{12}(y_n, u_{n_k}) \\ y_{n+1} = y_n + h\sum\limits_{k=1}^{s} b_k F(y_{n_k}, u_{n_k}), y(t_0) = y_0 \\ y_{n_k} = y_n + h\sum\limits_{j=1}^{s} a_k j F(y_{n_j}, u_{n_j}), k = 1, ..., s \\ k_1(y_n, u_{n_k}) \leq 0, \\ k_2(y_n, u_{n_k}) \geq 0, \end{cases}$$

when the following conditions are verified:

$$\begin{array}{ll} L_{y_n} & = \nabla_{y_n}(L_n + L_{n+1}) = 0 \\ L_{y_{n_k}} & = \nabla_{y_{n_k}} L_{n+1} = 0, k = 1, ..., s \\ L_{u_{n_k}} & = \nabla_{u_{n_k}} L_{n+1} = 10, k = 1, ..., s \\ L_{p_n} & = \nabla_{p_n} L_n = 0, n = 0, ..., N \\ L_{q_{n_k}} & = \nabla_{q_{n_k}} L_{n+1} = 0, k = 1, ..., s \end{array} \tag{18}$$

The Lagrangian L is given by the following formula:

$$\begin{array}{ll} L & = g(y_n, u_{n_k}) + L_0 + \sum\limits_{n=0}^{N-1} L_{n+1}, \\ L_0 & = p_0^T \left(y_(t_0) - y_0\right) \\ L_{n+1} & = p_{n+1}^T \left(y_n - y_{n+1} + h\sum\limits_{j=1}^{s} b_j F(u_{n_j}, y_{n_j})\right) + \\ & \sum\limits_{k=1}^{s} q_{n_k}^T \left(y_n - y_{n_k} + h\sum\limits_{j=1}^{s} a_{kj} F(u_{n_j}, y_{n_j})\right), n = 0, ..., N-1. \end{array} \tag{19}$$

Applying a symplectic partitioned Runge-Kutta method $M = (A, b), \tilde{M} =$

$(\tilde{A}, \tilde{b})$, we have:

$$
\begin{aligned}
&y_{n+1} = y_n + h\sum_{k=1}^{s} b_k \mathcal{H}_p(u_{n_k}, y_{n_k}), y(t_0) = y_0,\\
&y_{n_k} = y_n + h\sum_{j=1}^{s} a_{kj} \mathcal{H}_p(u_{n_j}, y_{n_j}), k = 1, .., s\\
&p_{n+1} = p_n - h\sum_{k=1}^{s} \tilde{b}_k \mathcal{H}_y(p_{n_k}, y_{n_k}), p_N = \phi'(t_f)\\
&p_{n_k} = p_n - h\sum_{j=1}^{s} \tilde{a}_{kj} \mathcal{H}_y(p_{n_j}, y_{n_j}),\\
&\mathcal{H}(y_{n_k}, p_{n_k}) = H(\psi(y_{n_k}, p_{n_k}), y_{n_k}, p_{n_k}),\\
&\tilde{a}_{kj} := b_j - \frac{b_j}{b_k} a_{jk}, b_j = \tilde{b}_j\\
&\\
&k_1(y_n, u_{n_k}) \leq 0,\\
&\\
&k_2(y_n, u_{n_k}) \geq 0.
\end{aligned}
\tag{20}
$$

Considering the numerical stream

$$
\begin{aligned}
&\xi_h : \mathbf{R^{2n}} \longrightarrow \mathbf{R^{2n}}\\
&(p_n, y_n) \longrightarrow (p_{n+1}, y_{n+1})
\end{aligned}
\tag{21}
$$

If the stream is selected such that the relation

$$
\left(\frac{\partial \xi_h}{\partial (p, y)}\right)^T \tilde{J} \left(\frac{\partial \xi_h}{\partial (p, y)}\right) = \tilde{J} \tag{22}
$$

is verified , the Runge-Kutta method is called symplectic for all regular Hamiltonian H and any integration step h. The characterization of the Runge-Kutta symplectic method is also done using the matrix $R = B\tilde{A} + A^T\tilde{B} - b\tilde{b}^T$ de $\mathbf{R^{2s}}$ when $B = diag(b_1, ..., b_s)$ and $\tilde{B} = diag(\tilde{b}_1, ..., \tilde{b}_s)$.

Partitioned symplectic Algorithm of Runge-Kutta (SPRK) .

1. Subdividing the interval time $[t_0, t_f]$ in N step $h = t_{n+1} - t_n = \frac{t_f - t_0}{N}$,N is the maximum number of iteration.

2. For $0 \leq n \leq N$,

$$
\begin{aligned}
&H_u(u_{ki}, y_{ki}, p_{ki}) = 0 \\
&y_{n+1} = y_n + h\sum_{k=1}^{s} b_k \mathcal{H}_p(u_{n_k}, y_{n_k}), y(t_0) = y_0, \\
&y_{n_k} = y_n + h\sum_{j=1}^{s} a_{kj} \mathcal{H}_p(u_{n_j}, y_{n_j}), k = 1, .., s \\
&p_{n+1} = p_n - h\sum_{k=1}^{s} \tilde{b}_k \mathcal{H}_y(p_{n_k}, y_{n_k}), p_N = \phi'(t_f) \\
&p_{n_k} = p_n - h\sum_{j=1}^{s} \tilde{a}_{kj} \mathcal{H}_y(p_{n_j}, y_{n_j}), \\
&\mathcal{H}(y_{n_k}, p_{n_k}) = H(\psi(y_{n_k}, p_{n_k}), y_{n_k}, p_{n_k}), \\
&\tilde{a}_{kj} := b_j - \frac{b_j}{b_k} a_{jk}, b_j = \tilde{b}_j \\
&k_1(y_n, u_{n_k}) \leq 0, \\
&k_2(y_n, u_{n_k}) \geq 0, \\
&Ecrire\ t_{n+1}, y_{n+1}, p_{n+1}.
\end{aligned}
\tag{23}
$$

3. Stop.

3.1 Calculation of order conditions of the SPRK algorithm.

The calculation of the order conditions of Runge-Kutta symplectic method is based on the graphs theory G_i (see annex) as shown by Julien Laurent-Varin in [18]. We first consider order conditions s=4, s=5. The table of the 91 conditions of order s = 6 [see annex].

Suppose that $d_j = \sum_i b_i a_{ij}, c_i = \sum_j a_{ij}, \tilde{b}_i = b_i, \sum_i b_i = 1, \sum_j d_j = 1, \sum_i c_j d_j = \frac{1}{6}, \sum_k \frac{1}{b_k} d_k^2 = \frac{1}{3}, \sum_i b_i c_i^2 = \frac{1}{3}$ the order conditions take the following form:

Table 1: SPRK order conditions equations, calculating the coefficients

Table of 8 order conditions when s=4			
Graph	Order Condition	Graph	Order Condition
G_1	$\sum_{l=1,k=1}^{4} \frac{1}{b_k} a_{lk} d_k d_l = \frac{1}{8}$	G_2	$\sum_{j=1,k=1}^{4} a_{jk} d_j c_k = \frac{1}{24}$
G_3	$\sum_{i=1,k=1}^{4} \frac{b_i}{b_k} a_{ik} c_i d_k = \frac{5}{24}$	G_4	$\sum_{i=1,j=1}^{4} b_i a_{ij} c_j = \frac{1}{8}$
G_5	$\sum_{j=1}^{4} c_j^2 d_j = \frac{1}{12}$	G_6	$\sum_{i=1}^{4} b_i c_i^3 = \frac{1}{4}$
G_7	$\sum_{k=1}^{4} \frac{1}{b_k} c_k d_k^2 = \frac{1}{12}$	G_8	$\sum_{l=1}^{4} \frac{1}{b_l^2} d_l^3 = \frac{1}{4}$

Table 2: SPRK order conditions equations, calculating the coefficients

Table of 27 order conditions, s=5			
Gs	Order Condition	Gs	Order Condition
G_1	$\sum_{i=1,k=1,l=1}^{5} \frac{b_i}{b_k} a_{ik} a_{il} d_k c_l = \frac{3}{40}$	G_2	$\sum_{i=1,k=1,j=1}^{5} b_i a_{ik} a_{ij} c_j c_k = \frac{1}{20}$
G_3	$\sum_{l=1,k=1,j=1}^{5} a_{lk} a_{kj} c_j d_l = \frac{1}{120}$	G_4	$\sum_{i=1,k=1,j=1}^{5} b_i a_{ik} a_{kj} c_i c_j = \frac{1}{30}$
G_5	$\sum_{i=1,k=1,l=1}^{5} \frac{b_i}{b_k} a_{lk} a_{il} c_i d_k = \frac{11}{120}$	G_6	$\sum_{l=1,i=1,k=1}^{5} \frac{b_i}{b_k} a_{lk} a_{ik} c_i d_l = \frac{3}{40}$
G_7	$\sum_{i=1,j=1,k=1}^{5} \frac{b_i b_j}{b_k} a_{jk} a_{ik} c_i c_j = \frac{2}{15}$	G_8	$\sum_{i=1,m=1,l=1}^{5} \frac{b_i}{b_l b_m} a_{im} a_{il} d_l d_m = \frac{2}{15}$
G_9	$\sum_{k=1,m=1,l=1}^{5} \frac{1}{b_k} a_{ml} a_{lk} d_k d_m = \frac{1}{30}$	G_10	$\sum_{k=1,m=1,l=1}^{5} \frac{1}{b_k} a_{mk} a_{lk} d_l d_m = \frac{1}{20}$
G_{11}	$\sum_{l=1,m=1}^{5} \frac{1}{b_l b_m} a_{lm} d_l^2 d_m = \frac{1}{15}$	G_{12}	$\sum_{k=1,l=1}^{5} \frac{1}{b_k} a_{kl} d_k^2 c_l = \frac{1}{60}$
G_{13}	$\sum_{l=1,m=1}^{5} \frac{1}{b_l^2} a_{ml} d_l^2 d_m = \frac{1}{10}$	G_{14}	$\sum_{i=1,l=1}^{5} \frac{b_i}{b_l^2} a_{il} c_i d_l^2 = \frac{3}{20}$
G_{15}	$\sum_{l=1,k=1}^{5} \frac{1}{b_k} a_{lk} d_k c_l d_l = \frac{7}{120}$	G_{16}	$\sum_{l=1,j=1,k=1}^{5} a_{jk} c_j d_j c_k = \frac{1}{40}$
G_{17}	$\sum_{l,k=1}^{5} \frac{1}{b_k} a_{lk} c_k d_k d_l = \frac{1}{40}$	G_{18}	$\sum_{i=1,k=1}^{5} \frac{b_i}{b_k} a_{ik} c_i c_k d_k = \frac{7}{120}$
G_{19}	$\sum_{i=1,k=1}^{5} \frac{b_i}{b_k} a_{ik} c_i^2 d_k = \frac{3}{20}$	G_{20}	$\sum_{i=1,j=1}^{5} b_i a_{ij} c_i^2 c_j = \frac{1}{10}$
G_{21}	$\sum_{k=1,j=1}^{5} a_{kj} c_j^2 d_k = \frac{1}{60}$	G_{22}	$\sum_{i=1,j=1}^{5} b_i a_{ij} c_i c_j^2 = \frac{1}{15}$
G_{23}	$\sum_{j=1}^{5} c_j^3 d_j = \frac{1}{20}$	G_{24}	$\sum_{i=1}^{5} b_i c_i^4 = \frac{1}{60}$
G_{25}	$\sum_{k=1,l=1}^{5} \frac{1}{b_k} c_k^2 d_l^2 = \frac{1}{30}$	G_{26}	$\sum_{l=1}^{5} \frac{1}{b_l^2} c_l d_l^2 = \frac{1}{20}$
G_{27}	$\sum_{m=1}^{5} \frac{1}{b_m^3} d_m^4 = \frac{1}{5}$		

4 Results and Discussion

Considering the 4 th order conditions for the practice of the SPRK algorithm, coefficients used and the numerically calculated are:

$$A = \begin{bmatrix} 1.3751 & 0.3171 & 0.5825 & -0.0241 \\ -0.0871 & -0.4950 & 0.0221 & -0.0303 \\ 0.5710 & 0.3226 & 0.1438 & 0.2943 \\ 1.0398 & -0.0127 & 0.1040 & -0.0516 \end{bmatrix}, \tag{24}$$

$$\begin{bmatrix} b \\ c \\ d \end{bmatrix} = \begin{bmatrix} 0.2131 & 0.5315 & 0.0698 & 0.1856 \\ 0.4996 & 0.4161 & -0.1896 & 1.0000 \\ 0.1065 & 0.3105 & 0.0830 & 0.0000 \end{bmatrix} \tag{25}$$

$$\tilde{A} = \begin{bmatrix} -1.1621 & -0.2595 & -0.1210 & 0.2066 \\ 0.2480 & 1.0266 & 0.0669 & 0.1962 \\ -1.5306 & -1.9258 & -0.0740 & -0.5973 \\ -0.9805 & 0.5678 & 0.0307 & 0.2372 \end{bmatrix}, \tag{26}$$

Table 3: Convergence order

Convergence order			
1.0e-06 *-0.0309	1.0e-06*-0.0148	1.0e-06 *-0.0350	1.0e-06 *-0.0142
1.0e-06 *-0.0000	1.0e-06*-0.0000	1.0e-06 *-0.0000	1.0e-06 * 0.0000
1.0e-06 * 0.0092	1.0e-06 *-0.0335	1.0e-06 *-0.0346	1.0e-06 *-0.1473
1.0e-06 * 0.0220	1.0e-06 *0.0030	1.0e-06 *0.0463	1.0e-06 *0.0826
1.0e-06 * 0.0000	1.0e-06 *0.0002	1.0e-06 *0.0006	1.0e-06 *-0.0376
1.0e-06 *0.0502	...	.....	.....

Where f_{val} means the precision of the obtained results.

5 Numeric Results

The following result are obtained with AMPL"A Mathematical Programming Modeling Language" and KNITRO.The final result precision is: Locally optimal solution found with final feasibility error (abs / rel) = 1.20e-07 / 2.19e-09 and final optimality error (abs / rel) = 1.69e-14 / 1.69e-14.

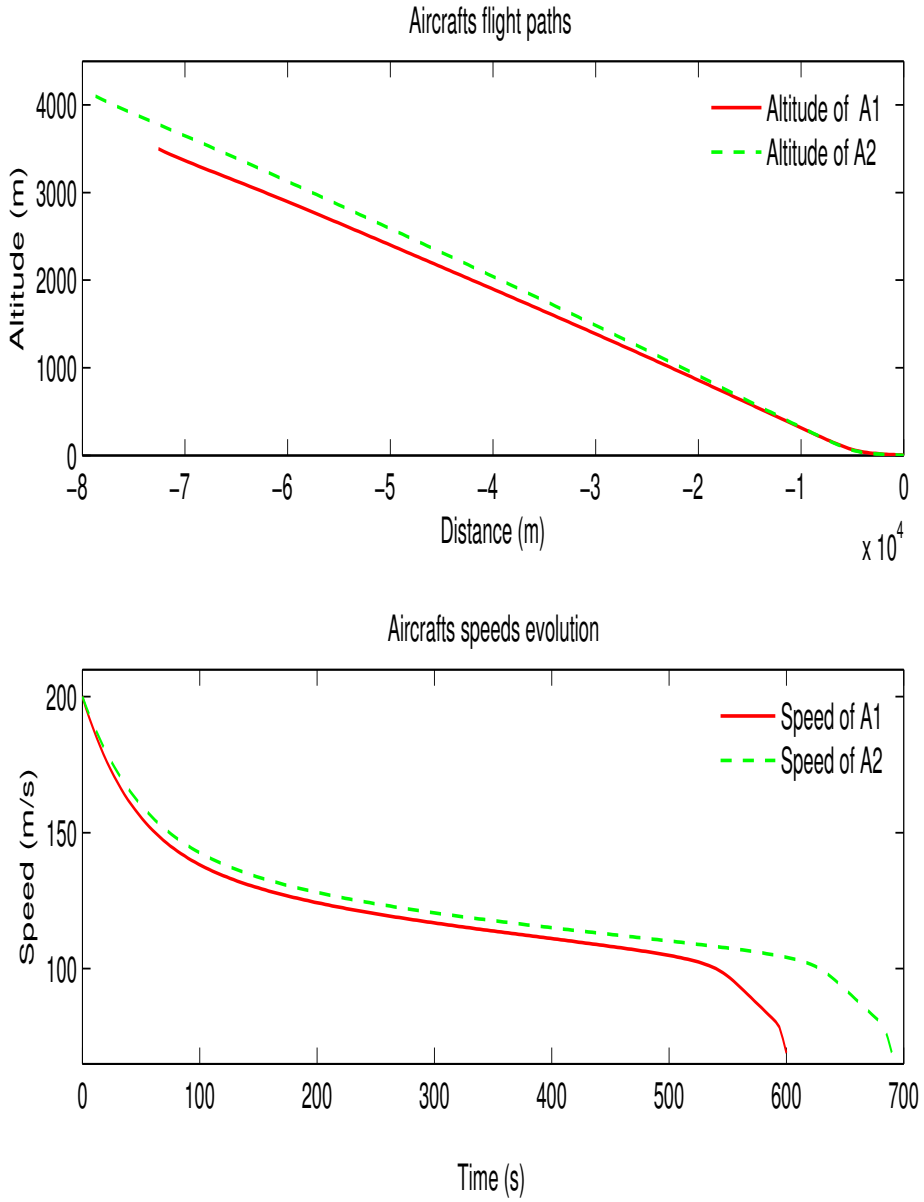

Figure 1: Two Aircraft flight paths and speeds

The above figure shows the continuous descent aircraft paths. When the first plane hit the ground, the second is six hundred m hight with a strike length of 3300 m. This result is therefore of constraints separation when the planes are landing successively on a single track. At the end of approach, both paths coincide and follow the standard Evolution of the path constructors data by the A300 aircraft. This figure also shows the evolution of the two

aircraft speeds and prove a landing because the speeds decrease from 200m/s up to 69 m/s as certified by ICAO and manufacturers of aircraft. Note that the touching ground speed is 69 m/s. These trajectories obtained are similar to the standard approach values as confirmed by Suzuki [19]

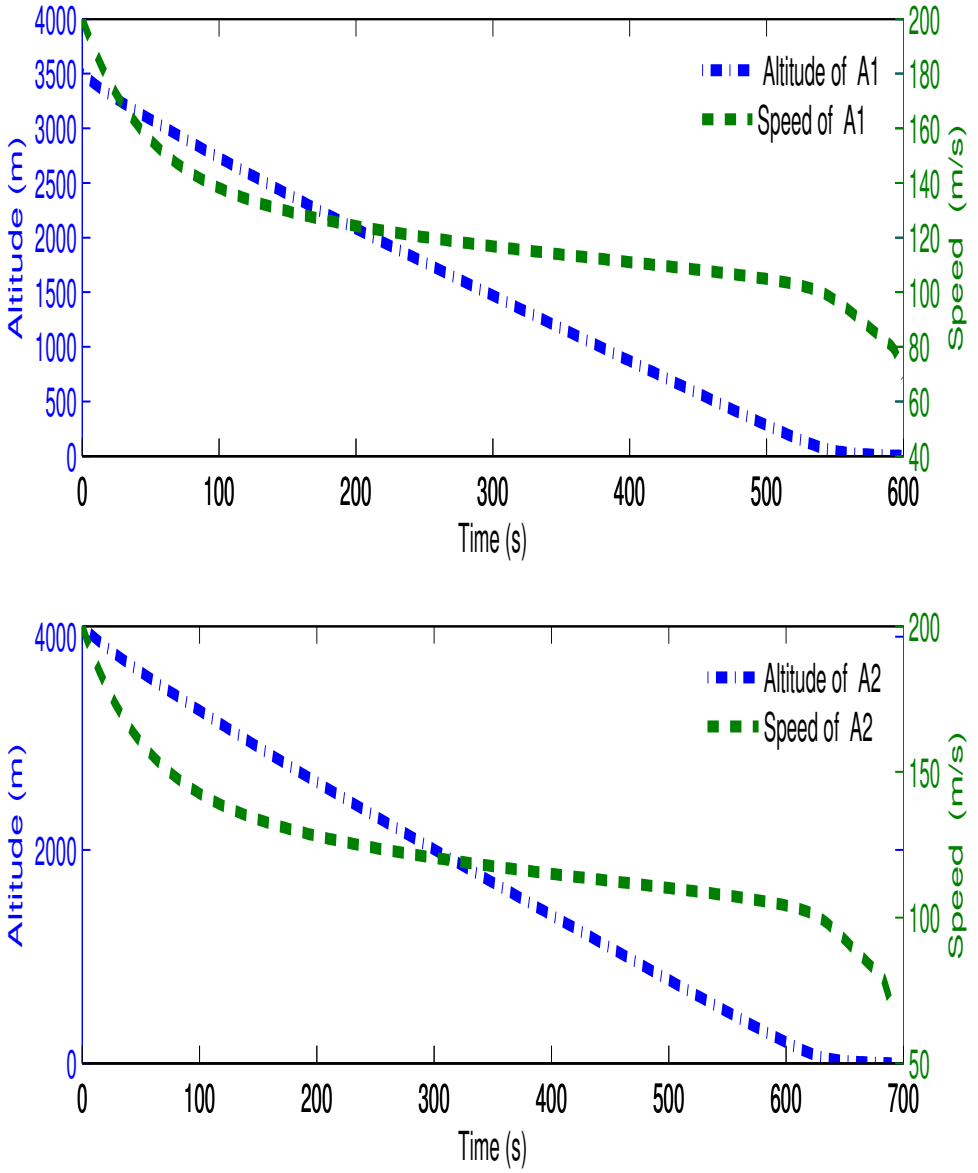

Figure 2: Evolutionary comparison of the trajectory and speed of each aircraft.

Figure 2 shows correlation between aircraft flight paths and speeds. The

maximum time of the approach is 600 seconds for the first aircraft and 690 seconds for the second, giving a separation time of 90 seconds.

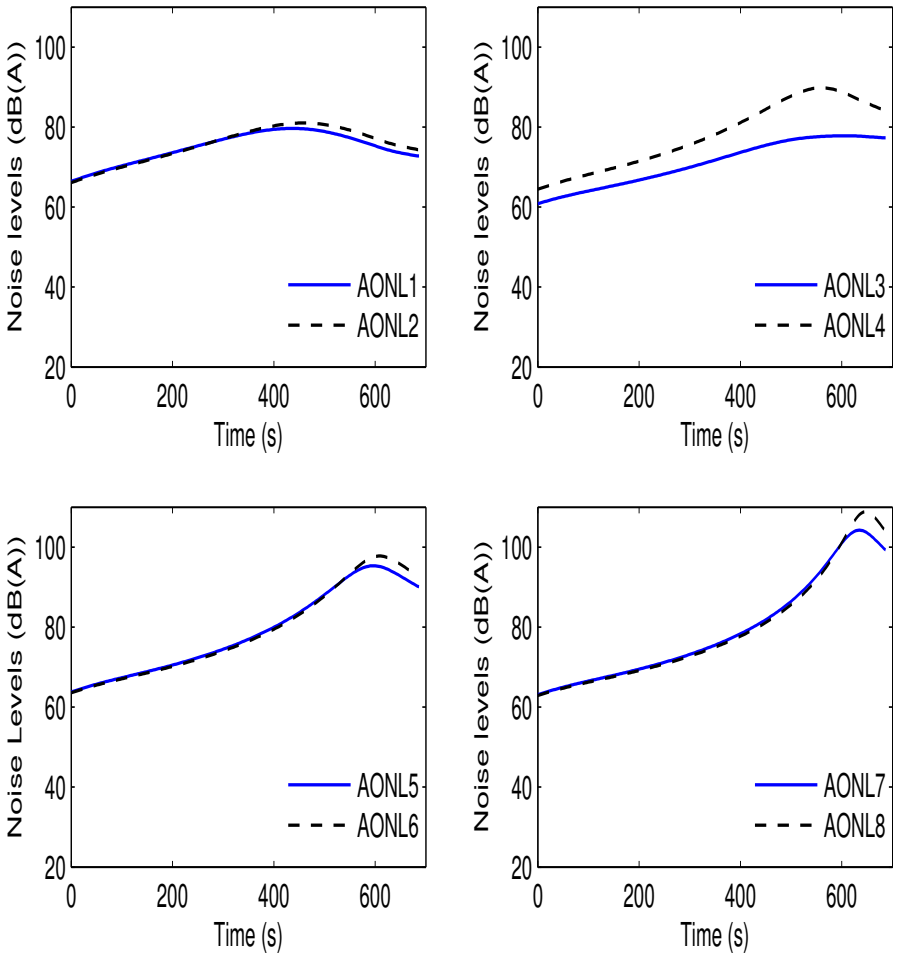

Figure 3: Noise emitted by the two-aircraft

Figure 3 shows the noise levels around airport when optimization is applied . This explains the importance of the acoustic optimization of approaching aircraft and gains brought by this model when compared with what is done daily. The observation position is considered on the ground below the path of the following way: $(-20000\ m, -20000\ m, 0\ m)$ for $AONL_1$, $(-19800\ m, -19800\ m, 0\ m)$ for $AONL_2$, ..., $(-\ 3200\ m, -3200\ m, 0\ m)$ to $AONL_8$. The touchdown point on the ground is $(0\ m, 0\ m, 0\ m)$ while the temporal separation of aircraft is 90 s. On each observation point, there is a vector of N noise levels as shown in discretization. It is important to consider

the maximum value among the N values, which value shows the shortest distance between the noise source and the observation point. This result shows that the maximum noise level varies depending on observation points and decreases when the plane moves away. By comparison, This result is close to the standard jet noise values approach as shown by Harvey[20, 21, 22, 23, 24, 25].

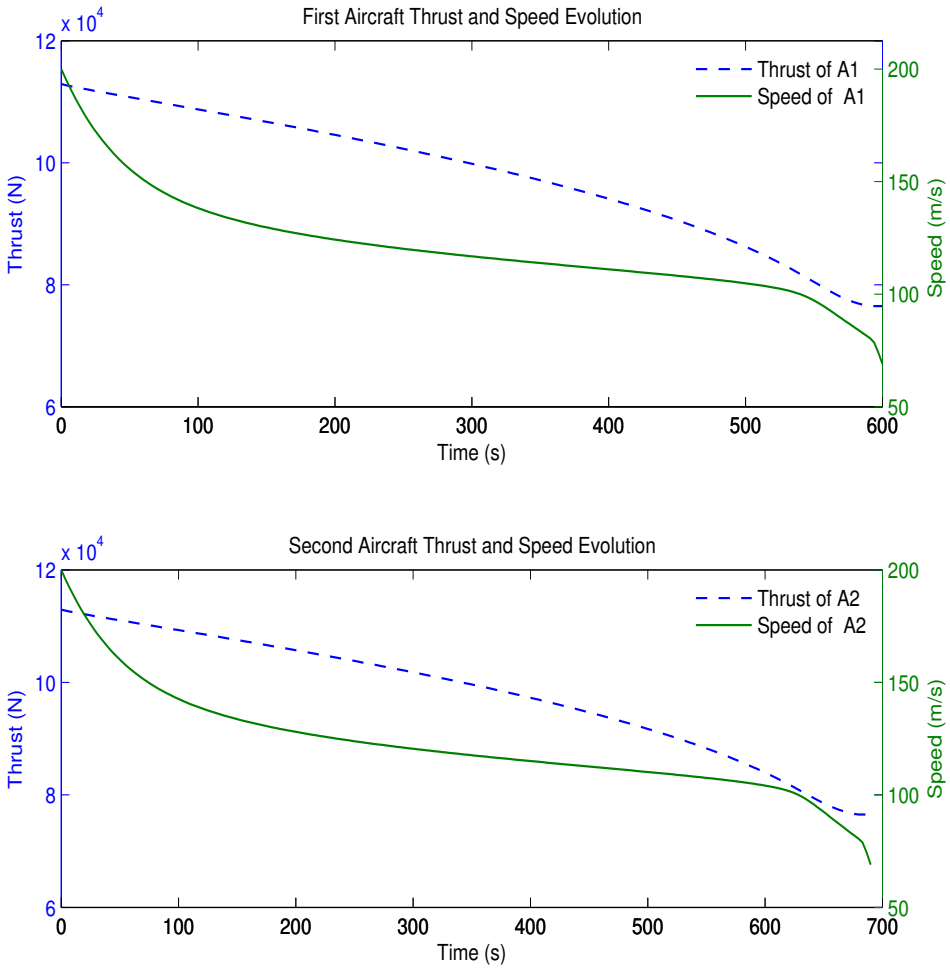

Figure 4: Comparing changes in thrust and speed of each aircraft

The figure 4 shows a simultaneous evolution of thrust and speed for each aircraft. It is noted that the speed decreases from 200 m / s to 69 m / s. Similarly, the thrust general trend is downward during landing. A correlation between the thrust and the speed of the two aircraft is very clarified.

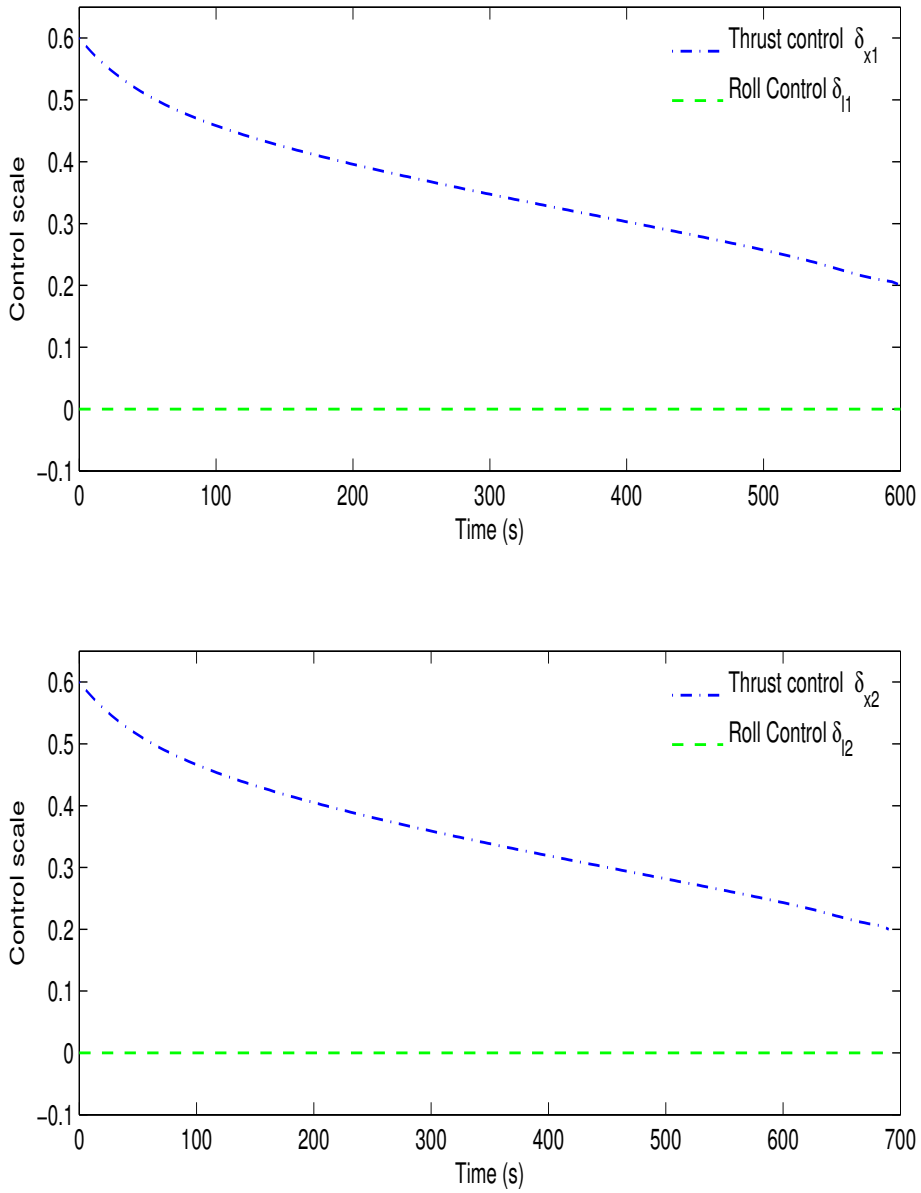

Figure 5: Aircraft Thrust and Roll control

The figure 5 shows the thrust control and the control roll caracteristics during landing. The main control of the aircraft varies from 0.6 to 0.2. The roll control remains zero, which proves stability of the aircraft and passengers comfort.

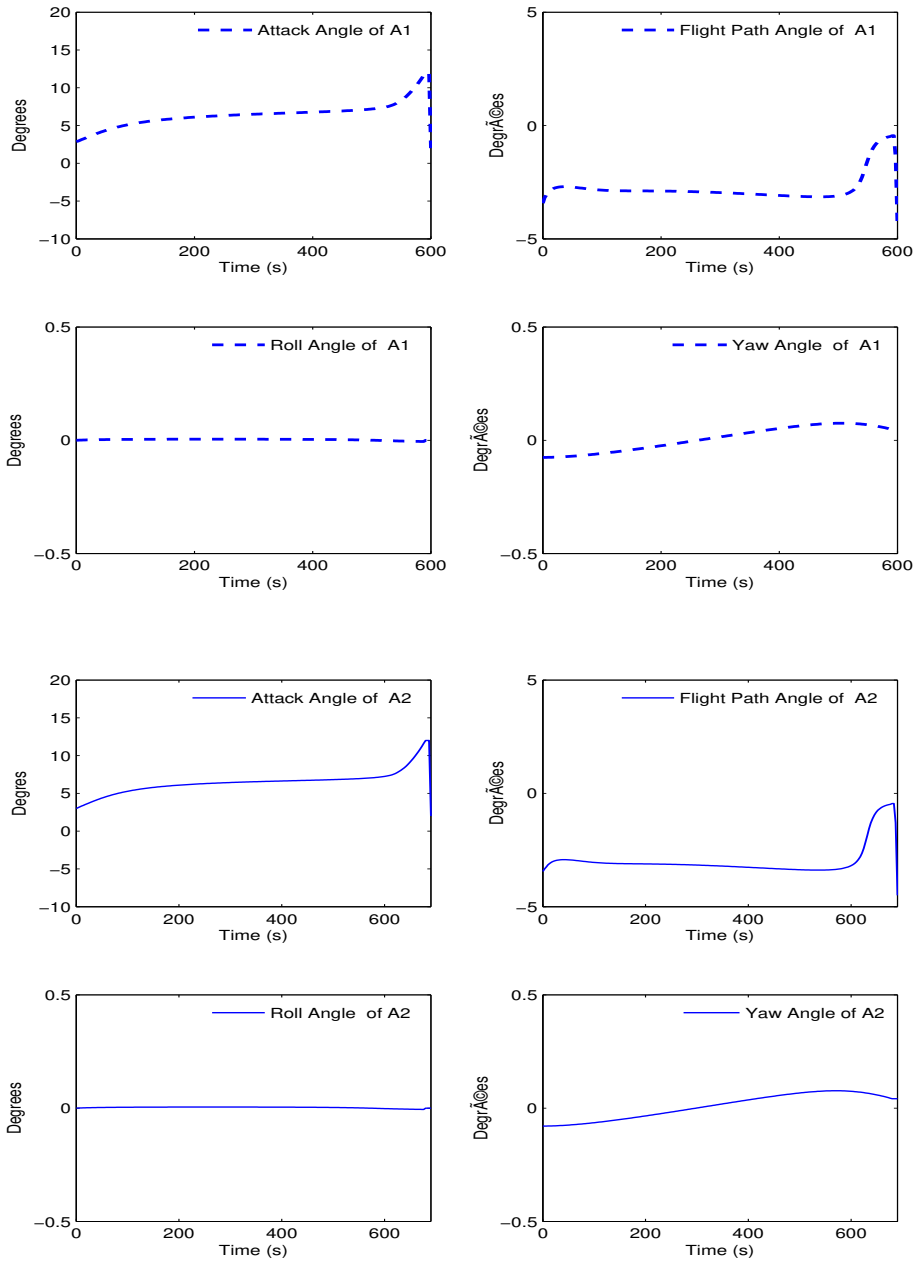

Figure 6: Evolution of aerodynamic angles of the two Aircrafts

This figure shows the evolution of the main aerodynamic angles of the two planes. It is clear that the roll is zero while the flight angle is negative throughout the landing as recommanded by ICAO in the approach procedures. The angle of attack varies between 2 and 12 degrees and the yaw angle is low because the plane is aligned to the runway.

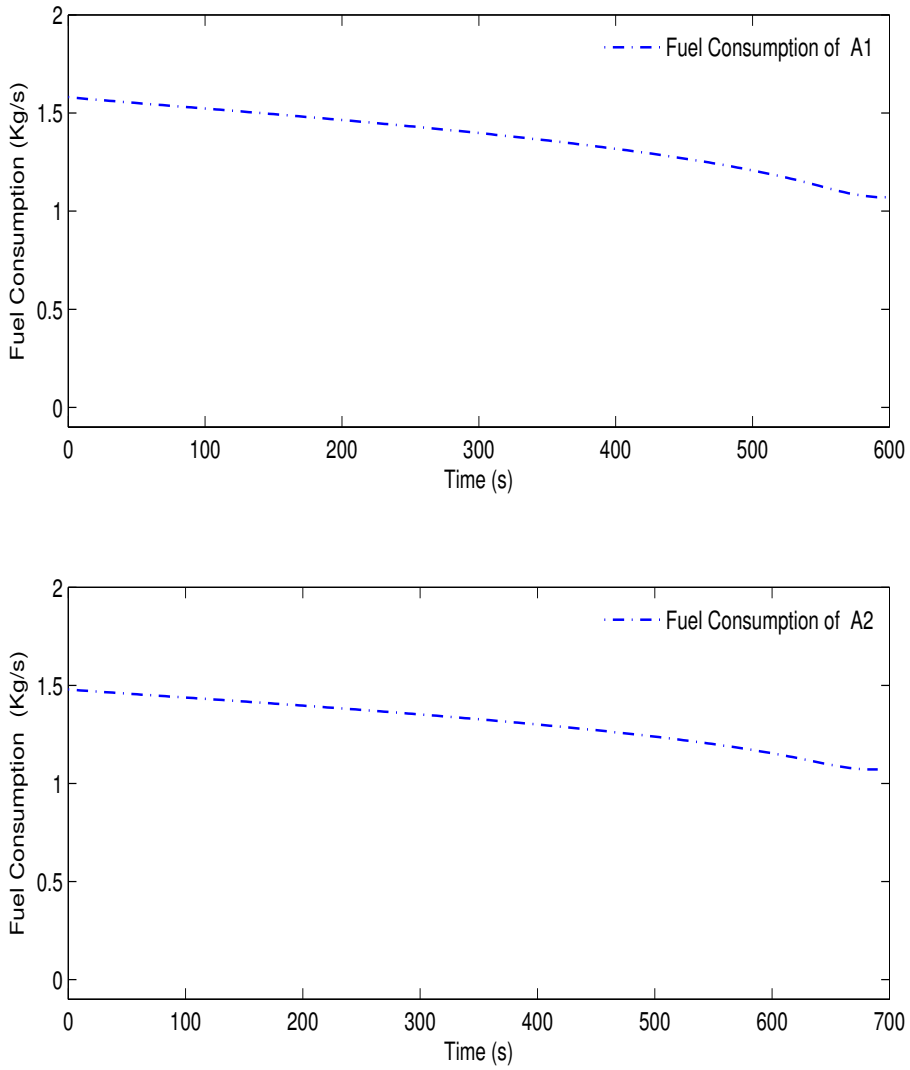

Figure 7: Evolution of kerosene usage of each Aircraft

The figure 7 shows the evolution of the consumption of kerosene by aircraft over time. It ranges from 1.5 kg / s to 1 kg / s on the ground. This result is already proven by Roux[15] and confirm the standars of the manufacturers of the A300 aircraft. Note that the base model operated in consumption is the Torenbeek one which has already proved its efficiency compared to other models.

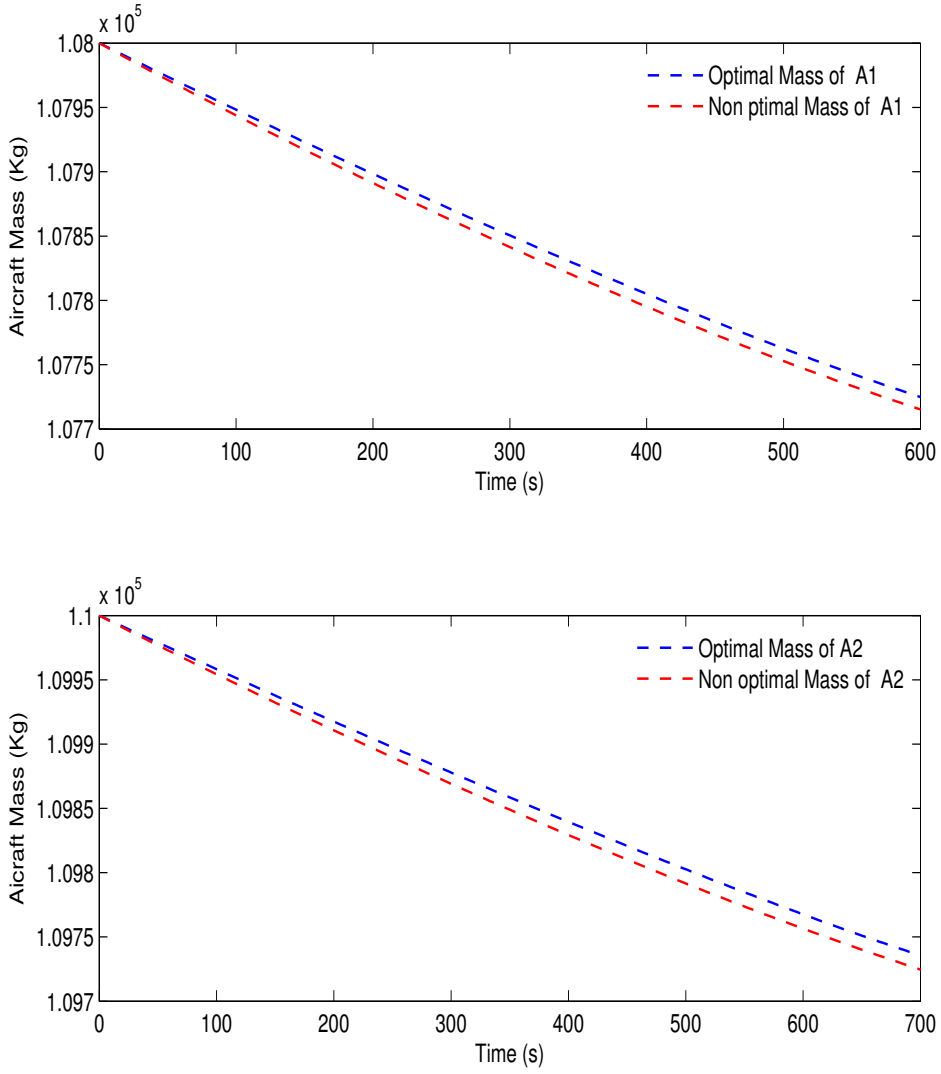

Figure 8: Evolution of the optimal mass and non optimal mass of each aircraft

The figure 8 shows the evolution of optimal and non optimal aircraft mass over time. In the first plane, the optimum mass varies from 108,000 kg to 107723.79176 kg on the ground while non optimal mass varies 108,000 kg 107714.15755 kg. For the second plane, the optimum mass varies from 110,000 kg to 109734.50191 kg on the ground when the non-optimal mass varies 110,000 kg to 109723.53824 kg. So it clears a weight saving between 9 kg and 11 kg.

6 Comparison of optimal procedures and standards

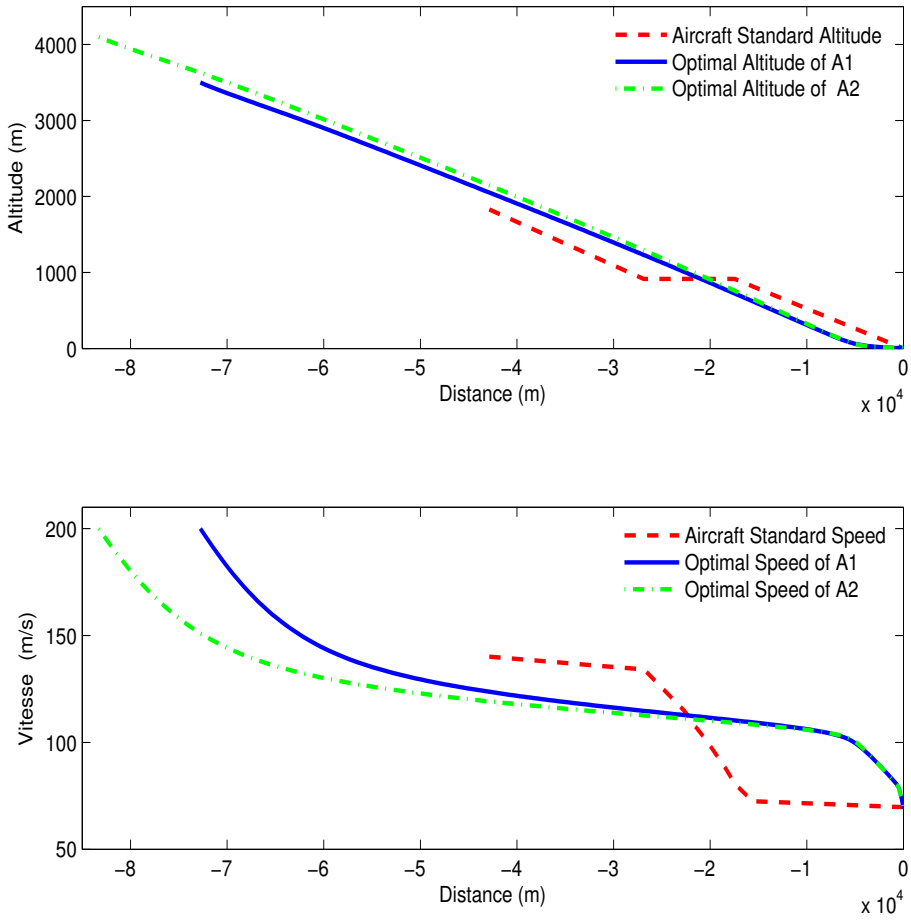

Figure 9: Comparison of optimal procedures and standards

The figure 9 shows the comparison of aircraft optimal procedures and standards. This is mainly the altitude and speed of the two approaching aircraft. It is clear that the continuous descent procedure well characterizes the optimal solution and that confirms the difference between the landing standard procedure and the landing optimal procedure. The optimal solution of the discrete problem found through a local convergence confirms the requirements of manufacturers and ICAO. Speed on the ground remains the same regardless of the particular proceedings and the slope of the path does not change.

7 Conclusion

In this paper, it was developed a numerical solution of optimal control problem in the case of two approaching aircraft. Theoretical and practical considerations of the SPRK algorithm are used for the establishment of a non-linear program, implementing the considered problem. The algorithm is based on the pontryaguin minimum principle to generate a search direction for all variables. An optimal solution of the discretized problem is found through a local convergence. The results show a reduction in noise and fuel consuption during the approach of two aircraft by considering several ground observers. The trajectories obtained have optimal characteristics and are acoustically effective. The numerical considerations used have no limitations except the introduction of the costate-variables without physical interpretation in order to facilitate the resolution of the dynamic system of two airplanes. The reason is the complexity of this system, which greatly affects the nature of the Solver to use. In this paper, the solver was chosen in consideration of all these parameters.
This model can be generalized for any type of aircraft when considering real case for air traffic and airport trafic.

Ackonwledgements

This article was supported by the Government of Burundi through the Ministry of Education, Higher Education and Scientific Research and the Ministry of Public Service, Labour and Employment.

References

[1] Peyrat-Armandy A., "Les avions de transport modernes et futurs", *Journal name*, TEKNEA, 1997.

[2] Martin D., "L'Analyse des Nuisances sonores autour des aéroports", *Revue technique numéro 58*, Mai 2000.

[3] Ventre M., *Les challenges environnementaux pour le transport aérien*, SAFRAN, Un leader technologique international, Septembre 2009.

[4] L. Abdallah., *Minimisation des bruits des avions commerciaux sous contraintes physiques et aérodynamiques*, Thèse de l'UCBL I, Septembre 2007.

[5] L. Abdallah, S. Khardi, and M. Haddou., *Optimization of operational aircraft parameters reducing noise emissions*, Laboratoire de Mathématiques et Applications, Physique Mathématique d'Orléans-Laboratoire Transport et Environnement(INRETS), France, 2008.

[6] K. Blin., *Stochastic conflict detection for air traffic management*, Eurocontrol Experimental centre Publications Office, France, April, 2000.

[7] C. Stoica., *Analyse, représentation et optimisation de la circulation des avions sur une plate-forme aéroportuaire*, Thèse de l'Institut national polytechnique de Toulouse-CNRS, France, Mai, 2005.

[8] J-F. Bonnans and J-L. Varin., *Computation of order conditions for symplectic partioned Runge-Kutta schemes with application to optimal control*, Numerische Mathematik, Springer-Verlag, September 2005.

[9] J-L. Boiffier, *The Dynamics of Flight, The Equations*, SUPAÉRO(Ecole Nationale Supérieure de l'Aéronautique et de l'Espace) et ONERA-CERT, Toulouse 25 Janvier 1999.

[10] DGAC, *Mémento à l'usage des utilisateurs des procédures d'approche et de départ aux instruments*, Rapport de la DGAC, 5ˆème édition, France, Août 1995.

[11] H. Sors, *Séparation et contrôle aérien*, International Virtual Aviation Organization[en ligne]disponible sur http://academy.ivao.aero/,15 octobre 2008.

[12] DGAC, *Méthodes et minimums de séparations des aéronefs aux procédures.*, Rapport de la DGAC, France, Fevrier 2009.

[13] E. Roux, *Modèle de longueur de piste au décollage-atterrissage, Avions de transport civil.*,SUPAERO-ONERA,2006

[14] Dominique O, *Cisaillement de vent ou Windshear.*,http://www.aviation-fr.info,2008

[15] E. Roux, *Pour une approche analytique de la dynamique du vol.*,Thèse-ONERA,Novembre 2005

[16] Boiffier J-L., *Dynamique de vol de l'avion.*,SupAéro, Départements des Aéronefs,Toulouse-Novembre 2001

[17] Ifrance, *Fiches techniques, historiques et photos d'avions A300-600, A300-600R [en ligne]disponible sur http://www.ifrance.com.*,SupAéro, Ifrance, France 2000

[18] J. LAURENT-VARIN, *Calcul des trajectoires optimales de lanceurs spatiaux réutilisables par une méthode de point intérieur.*,Thèse de l'Ecole polytechnique,France, Novembre 2005

[19] S. Suzuki T. Tsuchiya and A. Andreeva, *Trajectory Optimization for Safe, Clean and Quiet Flight.*,Dept. of Aeronautics and Astronautics, The University of Tokyo, ENRI International Workshop on ATM/CNS,Japan, EIWAC 2009

[20] H. Harvey Hubbard, *Aeroacoustics of flight vehicles, Theory and Practices.*,Volume 1: Noise sources and Volume 2: Noise Control. NASA Langley Research Center,Hampton, Virginia 1994

[21] F. Nahayo M.Haddou S.Khardi M.Hamadiche and J.Ndimubandi, *Two-Aircraft optimal control problem. The in-flight noise reduction.*,Journal of the European Series in Applied and Industrial Mathematics (ESAIM). Ed. EDP Sciences-ESAIM (Cambridge University press, USA),Mars, 2012

[22] S. Khardi, F. Nahayo, and M. Haddou, *The Trust Region Sequential Quadratic Programming Method Applied to two-Aircraft Acoustic Optimal Control Problem.*,Applied Mathematical Sciences, Vol.5, No.40, pp.1953-1976, 2011, ISSN 1312-885X

[23] F. Nahayo S.Khardi J.Ndimubandi M.Haddou and M.Hamadiche, *Two-Aircraft Acoustic Optimal Control Problem. SQP algorithms.*,ARIMA , Ed. INRIA, Vol.14., pp.101-123, France 2011

[24] F. Nahayo S. Khardi and M. Haddou, *Optimal control of two-commercial aircraft dynamic system during approach. The noise levels minimization.*,General Mathematics Notes, Vol.3 N°.2, April 2011

[25] M. Le Merrer, *Optimisation de trajectoire d'avion pour la prise en compte du bruit dans la gestion du vol.*,Thèse de l'ISAE, Département Onera : Commande des systèmes et dynamique du vol, campus SupAero, Toulouse, 18 janvier 2012